2005

Evaluation and Derivation of Cloud-Cover Algorithms for Calculation of Surface Irradiance in Sub-Antarctic and Antarctic Environments

Hae-Cheol Kim
Old Dominion University

Eileen E. Hofmann
Old Dominion University, ehofmann@odu.edu

Antarctic Science 17 (1): 135–150 (2005) © Antarctic Science Ltd Printed in the UK DOI: 10.1017/S0954102005002518

Evaluation and derivation of cloud-cover algorithms for calculation of surface irradiance in sub-Antarctic and Antarctic environments

HAE-CHEOL KIM* and EILEEN E. HOFMANN

Center for Coastal Physical Oceanography, Old Dominion University, Crittenton Hall, 768 W, 52nd Street, Norfolk, VA 23508, USA
** current address: Smithsonian Environmental Research Center, PO Box 28, 647 Contees Wharf Rd, Edgewater, MD 21037-0028, USA*
kimh@si.edu

Abstract: To investigate approaches for parameterizing cloud cover effects in models of surface irradiance, the daily-averaged and hourly irradiances measured at Palmer Station (64°46'S, 64°3'W), McMurdo Station (77°5l'S, 166°40'E) and Ushuaia (54°49'S, 68°19'W) between 1993 and 1997 were compared to irradiance values computed with a clear sky radiative transfer model in which nine empirical cloud-cover correction relationships were included. The cloud cover correction algorithms improved the simulated irradiance by factors of 3 and 3.7 for Palmer Station and Ushuaia, respectively, over the non-corrected irradiances. No single cloud cover correction algorithm worked consistently at the three sites. Therefore, a power function cloud cover correction algorithm was derived from comparisons between the observed spectrally-integrated irradiances and the simulated irradiances at the three locations. New coefficient values for the power function cloud cover correction algorithm for the spectrally-resolved irradiances were also derived at the three sites, and were found to be spectrally-neutral and to differ in magnitude. The general trends in the values obtained for the three sites provide an approach for generalizing cloud cover correction algorithm coefficients to other parts of the Antarctic.

Received 19 December 2003, accepted 1 October 2004

Key words: albedo, McMurdo Station, multiple reflection, Palmer Station, radiative transfer model

Introduction

Solar irradiance is an important input to models that are used to estimate marine primary production. Efforts to provide surface solar irradiance fields at a global scale from satellite-derived measurements have been made (Bishop & Rossow 1991, Bishop *et al.* 1997). However, such measurements are relatively recent and for some applications the resolution of the global scale irradiance fields is too coarse. Thus, radiative transfer (RT) models (Leckner 1978, Bird & Riordan 1985, Justus & Paris 1985, Green & Chai 1988, Gregg & Carder 1990) provide an alternative approach for estimating surface irradiance values. These models can be used to simulate irradiance values for remote locations over a wide range of space and time scales using a small number of meteorological input parameters that are relatively easy to obtain. Even without these input parameters, RT models can be implemented with standard atmospheric values that are representative of the meteorological conditions of a particular area (Davis 1995).

The RT models are based on a clear sky assumption. However, the attenuation of irradiance by cloud cover has more of an effect on the surface irradiance than any other meteorological variable. Also, in high latitude regions, the strongest departure from the one-dimensional assumptions on which the radiative transfer models are based comes from the spatial distribution of high-contrast ocean and snow-covered surfaces, which locally increase albedo effects. Thus, to obtain an accurate simulation of surface irradiance, it is necessary to account for cloud cover and albedo effects.

A limited number of empirically-derived cloud cover correction functions (Laevastu 1960, Tabata 1964, Reifsnyder & Lull 1965, Reed 1977, Kasten & Czeplak 1980, Dobson & Smith 1988, Davis 1995, Antoine & Morel 1996, Antoine *et al.* 1996), which are based on fractional cloud cover estimated using a two-dimensional cloud cover approximation, have been developed. However, the three-dimensional morphology of clouds affects the sea surface arriving irradiance (O'Hirok & Gautier 1998a, 1998b, Ricchiazzi & Gautier 1998, Ricchiazzi *et al.* 1998), which may explain discrepancies between the irradiances obtained using the two-dimensional approach and observational measures of atmospheric absorption. Moreover, the irradiance attenuation due to clouds is often approximated using monthly or seasonally-averaged cloud cover amounts, but the large spatial and temporal variability of clouds affects marine primary production at shorter time scales, such as diurnal.

Studies show that cloud cover can alter the spectral properties of the wave length-dependent downwelling irradiance, specifically in the ultraviolet and visible portions of the light spectrum (Spinhirne & Green 1978, Nann & Riordan 1990, Schafer *et al.* 1996, Seckmeyer *et al.* 1996,

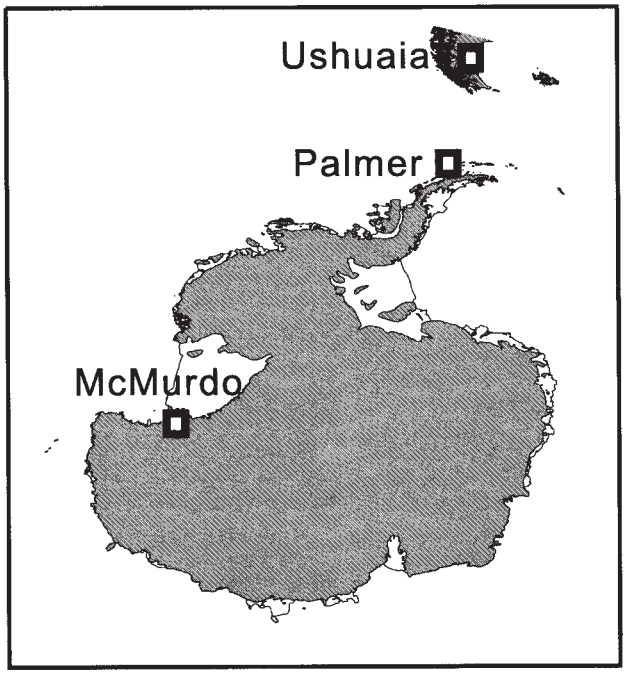

Fig. 1. Location map showing the three study sites: McMurdo Station (77°5l'S, 166°40'E), Palmer Station(64°46'S, 64°3'W) and Ushuaia (54°49'S, 68°19'W).

Bartlett *et al.* 1998, Siegel *et al.* 1999) and some attempts have been made to parameterize this effect (Siegel *et al.* 1999). Thus, the persistent cloud cover that frequently occurs in the Antarctic coastal areas has significant effects on the properties of the light arriving at the sea surface. Ozone depletion in the Antarctic atmosphere has allowed the amount of ultraviolet radiation, specifically ultraviolet-B (UV-B) radiation, reaching the sea surface to increase. Clouds also affect UV-B radiation and variations in cloud cover have more of an effect on the amount of this radiation reaching the sea surface than do variations in ozone (Gautier *et al.* 1994).

The objective of this study is to derive cloud cover correction algorithms for integrated and wavelength-resolved light spectra that are based on fractional cloud cover observations from two Antarctic sites, Palmer Station and McMurdo Station, and one sub-Antarctic site, Ushuaia (Fig. 1). The cloud cover relationships are used with a clear sky RT model to estimate the irradiance arriving at the surface at the three sites. The accuracy of the simulated surface irradiance, and hence the cloud cover algorithms, is determined by comparison to observed surface irradiance values from the three sites.

The models and datasets used in this study are described in the next section. This section also includes a discussion of existing cloud cover algorithms and presents new cloud cover algorithms derived for the three study sites. The simulated irradiance values are next described along with comparisons to observed values. The issues associated with application of cloud cover algorithms for high latitude sites are addressed in the discussion section. This section also discusses generalizations of the results of this study to derive cloud cover algorithms for Antarctic environments. The conclusion section suggests areas for future research.

Methods

Clear sky radiative transfer (RT) model

The RT model used in this study simulates the spectrally-dependent solar irradiance for clear sky conditions (Gregg & Carder 1990). This model is an extension of a continental aerosol model (Bird & Riordan 1985), which was modified to include maritime aerosol properties, irradiance transmittance through the air-sea interface, and atmospheric absorption of the light spectrum at 1 nm intervals (Gregg & Carder 1990). The RT model includes the range of 350–700 nm, with high spectral resolution, because of the importance of this part of the visible spectrum to phytoplankton growth and primary production (Gregg & Carder 1990).

In this study, the spectral range of the RT model was extended to 280 nm to include the ultraviolet region by using the extraterrestrial solar source function obtained from the Solar Ultraviolet Spectral Irradiance Monitor (SUSIM), which is a dual dispersion spectrometer aboard the Upper Atmosphere Research Satellite (UARS). Ozone absorption cross-sections were taken from Molina & Molina (1986) and are based on measurements at the lowest temperature (226 K) which reflects the cold Antarctic stratosphere. The temperature effect on ozone absorption cross-sections is significant for wavelengths longer than 280 nm (Molina & Molina 1986). Also, the effects of sea surface reflectance on irradiance and the contribution of the direct irradiance component resulting from multiple reflections between the ground (or sea surface) and air were included in the RT model, as described in Bartlett *et al.* (1998).

Table I. Definition and units of the terms and parameters used in Eqs (1–4).

Term/ parameter	Definition	Units
$F_0(\lambda)$	Mean extraterrestrial spectral irradiance	wm^{-2}
θ	Solar zenith angle	degree
$T_r(\lambda)$	Transmittance after Rayleigh scattering	none
$T_a(\lambda)$	Transmittance after aerosol scattering	none
$T_{0Z}(\lambda)$	Transmittance after ozone absorption	none
$T_0(\lambda)$	Transmittance after oxygen absorption	none
$T_W(\lambda)$	Transmittance after water vapour absorption	none
ρ_d	Direct sea surface reflectance	none
ρ_s	Diffuse reflectance	none
$I_r(\lambda)$	Diffuse irradiance component from Rayleigh scattering	$wm^{-2}nm^{-1}$
$I_a(\lambda)$	Diffuse irradiance component from aerosol scattering	$wm^{-2}nm^{-1}$
r_s	Clear-sky reflectivity (albedo)	none
r_g	Ground reflectivity (albedo)	none

Table II. Definitions and values of the input parameters used with the clear sky RT model at the three sites. Default values were used for parameters for which measurements were not available. The input parameters used for sensitivity studies are shown in bold type.

Input parameter	McMurdo	Palmer	Ushuaia
Solar zenith angle (°)	55.72–87.99	41.21–87.95	31.48–87.98
Latitude	77°51'S	64°46'S	54°49'S
Longitude	166°40'E	64° 3'W	68°19'W
Barometric pressure (mbar)	913–1090	953–1017	957–1033
Local wind speed (ms^{-1})	0–36	0–33	0–39
Visibility (km)	0.5–72	0.1–72	0.1–72
Ozone (Dobson Unit)	111–413	132–405	158–403
Reflectivity (tenth)	0.3–0.99	0.07–0.99	0.05–0.99
Mean wind speed (ms^{-1})	0–28.2	0–23.5	0–13.3
Air mass type	Marine type (1)	Marine type (1)	Marine type (1)
Relative humidity (%)	80 (Default)	46–100	23–100
Water vapour (cm)	1.5 (Default)	1.5 (Default)	1.5 (Default)

The governing equations for the modified RT model are:

$$E_{dd}(0^-,\lambda) = F_0(\lambda)\cdot\cos\theta\cdot T_r(\lambda)\cdot T_a(\lambda)\cdot T_{oz}(\lambda)\cdot T_o(\lambda)\cdot T_w(\lambda)\cdot(1-\rho_d) \quad (1)$$

$$I_g(\lambda) = (E_{dd} + I_r + I_a)\, r_s r_g / (1 - r_s r_g) \quad (2)$$

$$E_{ds}(0^-,\lambda) = [I_r(\lambda) + I_a(\lambda) + I_g(\lambda)]\cdot(1-\rho_s) \quad (3)$$

$$E_d(0^-,\lambda) = E_{dd}(0^-,\lambda) + E_{ds}(0^-,\lambda) \quad (4)$$

where Eqs (1–4) give the direct component of downwelling irradiance ($E_{dd}(0^-, \lambda)$) just beneath the sea surface (0^-) for each wavelength (λ), the diffuse irradiance component arising from multiple ground-air interactions ($I_g(\lambda)$), the diffuse component of downwelling irradiance just beneath the sea surface ($E_{ds}(0^-, \lambda)$), and the down-welling irradiance just below the sea surface ($E_d(0^-, \lambda)$), respectively. All values are expressed in W m^{-2} nm^{-1}. All terms and parameters used in Eqs (1–4) are defined in Table I.

The direct component of downwelling irradiance (Eq. 1) is calculated from the mean extraterrestrial spectral irradiance which is modified by various scattering, absorption and reflectance processes. The effect of multiple air-ground reflections (Eq. 2) is determined from the influence of the sky and ground albedos on the direct component of downwelling irradiance. The diffuse component of the downwelling irradiance (Eq. 3) is

Table III. Equation, source and region of application for the nine cloud cover correction algorithms used with the clear sky RT model. The fractional change in irradiance is computed from the irradiance from the clear sky model, E_m, and the irradiance under cloudy conditions, E_c. Both values are in W m^{-2}. Parameters input to the algorithms are cloud tenths (C_{ten})) cloud oktas (C_{okt}), solar elevation (α), and the fraction of the total radiation in the photosynthetically active radiation range (F_{vis}).

Cloud cover correction algorithm	Source	Region of application
$\frac{E_c}{E_m} = 10^{-0.99C_{ten}}$	Reifsnyder & Lull 1965	Southeastern Forest, USA
$\frac{E_c}{E_m} = 1 - 0.75\left(\frac{C_{okt}}{8}\right)^{3.4}$	Kasten & Czeplak 1980	Hamburg, Germany
$\frac{E_c}{E_m} = 1 - 0.674C_{ten}^{2.854}$	Davis 1995	Seattle-Tacoma airport, USA
$\frac{E_c}{E_m} = 1 - 0.632C_{ten} + 0.0019\alpha$	Reed 1977	Swan Island, Carribean; Cape Hatteras & Astoria, USA
$\frac{E_c}{E_m} = 1 - 0.6C_{ten}^3$	Laevastu 1960	Ocean Station P
$\frac{E_c}{E_m} = 1 - 0.716C_{ten} + 0.00252\alpha$	Tahata 1964	Ocean Station P
$\frac{E_c}{E_m} = 1 - 0.53\sqrt{C_{ten}}$	Dobson & Smith 1988	Ocean Station P & Sable Island
$\frac{E_c}{E_m} = 1 - \frac{0.75(1 - 0.632C_{ten} + 0.0019\alpha)}{1 - 0.25F_{vis}}$	Antoine & Morel 1996 (modified Reed 1977)	World Ocean
$\frac{E_c}{E_m} = 1 - 0.29\left(C_{ten} + C_{ten}^2\right)$	Antoine *et al.* 1996	World Ocean

determined from scattering and reflectance processes. Equation (4) is the sum of the direct and diffuse components of the downwelling irradiance which is the downwelling irradiance just below the sea surface. In this study, the simulated irradiance values were compared to land-based observed irradiance values ($E_d(0^+, \lambda)$)from three sites. As a result, the effect of sea surface reflectance on the direct [$(1 - \rho_d)$ in Eq. (1)] and diffuse [$(1 - \rho_s)$ in Eq. (3)] irradiance components was not included.

Input data for RT model

The clear sky RT model requires a number of input parameters that can either be measured or calculated (Table II). Solar zenith angle is related to the astronomical position of the Earth, and can be calculated from Julian day, Universal Time Coordinate (UTC), latitude, and longitude. Barometric pressure, local wind speed, visibility, ozone, and reflectivity measurements, were obtained from *in situ* measurements made at land-based weather stations or from satellites. Relative humidity was calculated from dew point and dry temperatures measured at the weather stations. The mean wind speed was calculated from measurements of local wind speed at the study sites. Air mass type is defined by ten categories that range from typical open ocean aerosol with a value of 1.0 to typical continental aerosol with a value of 10. For this study, air mass type was assumed to be typical open ocean aerosol because the three sites are located near the coastal ocean. The default water vapour value was used *in lieu* of actual measurements. Water vapour (Table II) represents total precipitable water in a 1 cm^2 area in a vertical path from the top of the atmosphere to the surface (Gregg & Carder 1990).

Cloud correction algorithms

Nine empirical cloud cover algorithms (Table III) were tested with the clear sky RT model to determine their effect on the sea surface arriving irradiance. The existing cloud cover algorithms were developed for a range of environments that include a forest area in mid-latitude United States (Reifsnyder & Lull 1965), northern Germany (Kasten & Czeplak 1980), the north-western United States (Davis 1995), and sites along the east and west coasts of the United States (Reed 1977). Three cloud cover algorithms were developed for open ocean environments that include Ocean Weather Station Papa and Sable Island (Laevastu 1960, Tabata 1964, Dobson & Smith 1988). Two cloud cover algorithms were developed for a global application (Antoine & Morel 1996, Antoine *et al.* 1996). With the exception of the algorithm developed by Kasten & Czeplak (1980), which is based on cloud oktas, all cloud cover algorithms are based on cloud tenths.

Irradiance data

The United States National Science Foundation supports a network of ultraviolet spectroradiometers (SUV-100), which are manufactured by Biospherical Instruments Inc. This network provides time series measurements of the incident radiant flux ($\mu W\ nm^{-1}cm^{-2}$) at sites in the Antarctic and sub-Antarctic. For this study, the measured irradiance time series were obtained from 1993 to 1997 at Palmer Station, McMurdo Station and Ushuaia (Fig. 1). The irradiance data have a spectral irradiance resolution of 1 nm between 280 nm and 620 nm and are available at 1-hour intervals (Booth *et al.* 1998, 2000, 2001). The irradiance time series were daily averaged and these values, as well as the hourly values, were used for comparison with the simulated irradiance values obtained with the clear sky RT model.

Cloud cover is defined by the World Meteorological Organization (WMO) Code 2700 to be the fraction of the total sky covered by clouds. Cloud cover observations are generally available at the study sites every three hours, with occasional missing observations. In this study, the missing values were not obtained by interpolation between the available cloud cover measurements because synoptic cloud cover can change radically on short timescales. All the analyses were done with only those surface irradiance measurements that have cloud cover observations that match precisely in time.

Concurrent meteorological observations, such as barometric pressure, wind speed, visibility, and relative humidity are available from the National Climatic Data Center (NCDC) weather observations and are provided along with the irradiance data from Biospherical Instruments Inc. (Booth *et al.* 1998, 2000). Global measurements of total column ozone are provided by National Aeronautics and Space Administration (NASA) Total Ozone Mapping Spectrometer (TOMS) instruments. The Meteor-3 TOMS provided daily data from November 1978–December 1994, and the Earth Probe TOMS has been providing data since July 1996 (Booth *et al.* 1998, 2000). In the present study, the Meteor-3 TOMS data was used for input data between 1993 and 1994 and Earth Probe TOMS data was used for input data between 1996 and 1997. Climatological values for column ozone data were used for one-half years between 1995 and 1996, when satellite measurements were not available. The number of random errors, decode errors, and reporting errors (by Station) is less than 0.1% of the total observations (NCDC 2003).

Simulations and sensitivity studies

The sensitivity of the simulated irradiances to six meteorological parameters, barometric pressure, wind speed, visibility, ozone concentration, ground albedo (reflectivity), and relative humidity, was evaluated. The

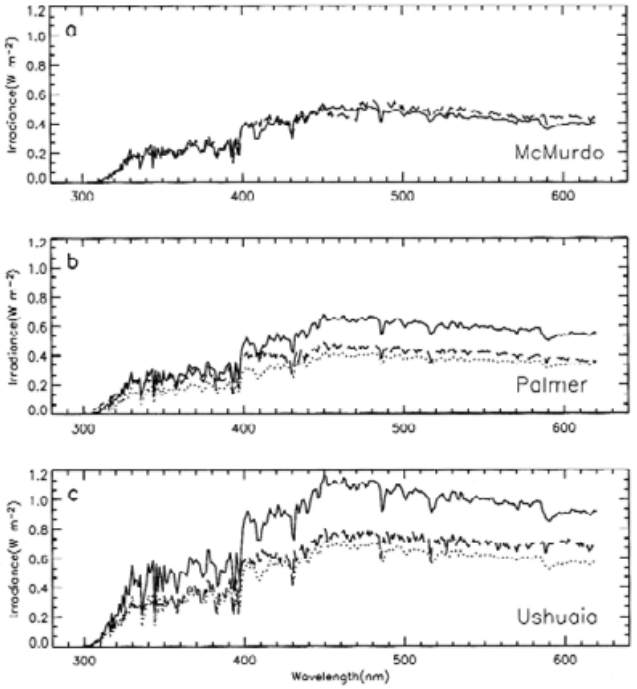

Fig. 2. Comparison between observed (– – –) and simulated (—) irradiances at **a.** McMurdo Station, **b.** Palmer Station, and **c.** Ushuaia for 9 November 1994, 19 October 1995, and 13 November 1994, respectively. The simulated hourly irradiances were calculated based on temporal and meteorological information that is concurrent with the observed irradiance measurements. The simulated and observed hourly irradiance data were averaged over the number of observations to obtain daily mean irradiance values. The simulated irradiance obtained for Palmer Station and Ushuaia from the RT transfer model that included a cloud cover correction algorithm (Antoine *et al.* 1996) is shown by the dotted line.

sensitivity studies were done using the maximum and minimum values of the six meteorological input parameters with all other parameters held constant. The sensitivity of the simulated irradiances to changes in the input parameters was evaluated by comparison to the irradiances obtained from the clear sky RT model using measures of magnitude and consistency changes based on percent root mean square (RMS) difference and Spearman's ranked correlation coefficient, respectively. This provides a measure of which meteorological parameters have the most effect on the magnitude and shape of the simulated irradiances.

Results

Simulation of daily-averaged irradiance

A comparison between observed and simulated irradiances obtained from the clear sky model at the three sites for a particular time (Fig. 2) shows that the spectral shape of the two are similar. The average correlation coefficients (r^2) obtained for the comparison between the simulated and observed irradiances were 0.97, 0.96, and 0.95 for McMurdo Station, Palmer Station and Ushuaia, respectively. However, at McMurdo Station (Fig. 2a) the observed irradiances are greater than the theoretical maximum obtained from the clear sky model, which suggests a strong albedo effect at this site. At Palmer Station and Ushuaia (Fig. 2b & c) the magnitude of the observed irradiance is less than that derived from the clear sky model because of the effect of cloud cover. The patterns shown for austral spring (Fig. 2) for the three sites were consistent for the simulations done with the RT model for other times. However, the differences in magnitude between the observed irradiances and those derived from the clear sky model indicate the need to correct the simulated values for cloud cover and local albedo effects.

Table IV. Percentage of days at each site for which the RMS difference between the simulated and observed irradiances was less than 20% for the RT model with no cloud cover correction and for each cloud cover algorithm.

Algorithm	McMurdo	Palmer	Ushuaia
Without correction	57	12	15
Reifsnyder & Lull 1965	1	3	1
Kasten & Czeplak 1980	51	21	48
Davis 1995	47	28	53
Reed 1977	36	33	55
Laevastu 1960	62	29	42
Tabata 1964	28	36	56
Dobson & Smith 1988	19	31	48
Antoine & Morel 1996 (modified Reed 1977)	16	33	18
Antoine *et al.* 1996	46	34	56

The nine cloud cover correction algorithms (cf. Table II) were applied to the simulated irradiances obtained from the clear sky RT and the simulated values were assumed to be improved if an algorithm resulted in a RMS difference between the observed and corrected irradiances for a given day of < 20%, and a correlation coefficient between the two of more than 90% with a significance (P) value of < 0.05. The percentage of the available days on which these conditions were met was calculated and compared to the percentage of days from the uncorrected clear sky model that satisfied these conditions (Table IV). The reliability of a particular cloud cover algorithm was determined by the increase in the percentage of days with good comparisons with observations relative to the uncorrected model output. A total 590 days of irradiance data, distributed as 183 days at McMurdo Station, 195 days at Palmer Station and 212 days at Ushuaia, all from the spring and summer were used in this daily-averaged irradiance comparison study.

At McMurdo Station, none of the cloud cover correction algorithms provided a significant improvement in the simulated irradiances, relative to the non-corrected irradiance values (Table IV). In fact, many of the cloud cover algorithms actually resulted in degrading the simulated irradiances relative to those obtained from the non-corrected clear sky model. At Palmer Station, the cloud

Table V. Sensitivity of the irradiance simulations to certain input parameters expressed as percent RMS difference and ranked correlation coefficient (values in parentheses) at each site. The percent RMS difference gives the correspondence between the simulated irradiance obtained from the clear sky RT model and that obtained from the model with the modified parameter set. The ranked correlation coefficient provides a measure of the consistency between the two simulated irradiance distributions. As only one default value was used for the relative humidity at McMurdo, the sensitivity to this input parameter was not tested.

Parameter	McMurdo	Palmer	Ushuaia
Barometric pressure	1.33 (1.0)	0.58 (1.0)	0.91 (1.0)
Local wind speed	0.03 (1.0)	0.02 (1.0)	0.03 (1.0)
Visibility	24.63 (0.99)	21.21 (0.99)	22.98 (0.99)
Ozone	11.20 (0.95)	4.28 (0.99)	3.77 (0.99)
Reflectivity (albedo)	20.96 (0.92)	14.47 (0.97)	16.70 (0.96)
Relative humidity (%)	-	1.74 (1.0)	2.33 (1.0)

cover algorithms by Tabata (1964), Reed (1977), Dobson & Smith (1988), Antoine & Morel (1996), and Antoine *et al.* (1996) resulted in a three-fold improvement in the percentage of days on which the simulated irradiances matched observations. At Ushuaia, six of the cloud cover algorithms resulted in substantial improvement in the simulated irradiance values. However, those by Tabata (1964) and Antoine *et al.* (1996) gave about a 57% improvement relative to the uncorrected clear sky model results. The cloud cover algorithm by Reifsnyder & Lull (1965) underestimated the cloud-cover filtered irradiance at all sites tested and as a result made the comparisons between simulated and observed irradiances poorer. Application of the Antoine *et al.* (1996) algorithm to the irradiances derived from the clear sky model at Palmer Station and Ushuaia resulted in corrected irradiance values that match observations (dotted line, Fig. 2b & c) and the overall spectral shape after correction followed the observations at both sites.

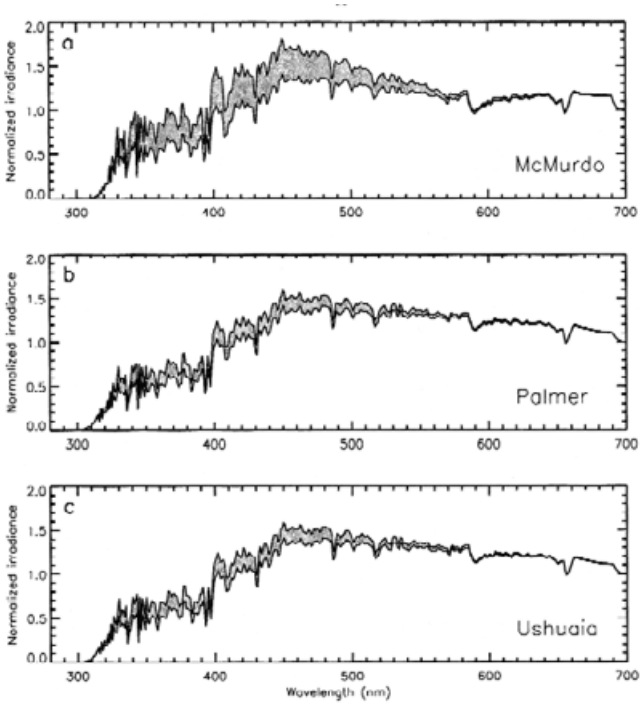

Fig. 3. Comparison of the effect of variations in reflectivity between a minimum of 0 and a maximum of 0.9 on simulated irradiances obtained from the clear sky model for **a.** McMurdo Station, **b.** Palmer Station, and **c.** Ushuaia. The whole irradiance spectra was normalized by the irradiance at 700 nm. The shaded region shows the range of variation due to changes in reflectivity.

Input parameter sensitivity studies

The clear sky model contains many input parameters that affect the value and spectral shape of the simulated irradiances. Therefore, the sensitivity of the simulated irradiances to the six primary input parameters was tested (Table V). For each sensitivity test, the parameters not being varied were specified with mean values. Default values were used for water vapour.

Of the six parameters tested, variations in visibility and reflectivity (ground albedo) were found to be most influential on the simulated irradiances at the three sites (Table V). The percent RMS difference between the simulated irradiances obtained using the maximum and minimum reflectivity was about 14–21%. Variations in visibility changed the irradiance values by 21–25%. Ozone concentration variation also has an effect, changing irradiances by 4–11%. If these meteorological conditions are assumed to be representative of Antarctic environments then reflectivity, visibility, and ozone are the three input parameters that have the most effect on irradiance. Assuming the range of reflectivity variation and visibility are similar for the three sites, the effect of reflectivity on irradiance was more significant at McMurdo Station than the effect of visibility. The effect of variations in reflectivity on simulated irradiance is largest at McMurdo Station (Fig. 3a), with a RMS difference between the maximum (0.01) and minimum values (0.9) of 25%. This is as expected given the high latitude of this site. The effect of reflectivity variations at Palmer Station (Fig. 3b) and Ushuaia (Fig. 3c) is less but it is still within the range of variation observed for comparisons between observed irradiances and those obtained with a cloud cover correction algorithm (cf. Fig. 2).

Derivation of new algorithms for integrated irradiance (280–620 nm)

The cloud cover correction algorithms by Laevastu (1960), Kasten & Czeplak (1980), Dobson & Smith (1988), and Davis (1995) are of the general form:

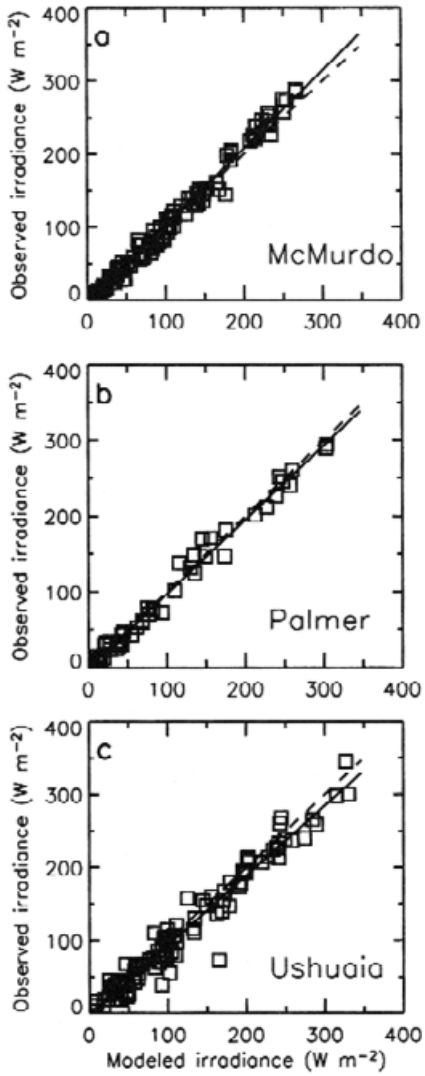

Fig. 4. Comparison between the observed and simulated spectrally-integrated irradiances for clear sky conditions for **a.** McMurdo Station, **b.** Palmer Station, and **c.** Ushuaia. The irradiance values were integrated over 280 to 620 nm. The linear regression between the observed and simulated irradiances is given by the solid line and the 1:1 correspondence line, given for reference, is shown as a dashed line. The slope and constant for the linear relationship were 1.07, -570 for McMurdo station, 0.98, -72 for Palmer station, and 0.96, -255 for Ushuaia, respectively.

$$\frac{E_{obs}}{E_{clear}} = 1 - A \cdot (CLD)^{B} \qquad (5)$$

where the coefficients A and B are dimensionless parameters that determine the shape and the magnitude of the cloud-cover correction algorithm, respectively. The degree of cloudiness, expressed in either tenths or oktas, is given by CLD. For clear sky conditions the ratio $\frac{E_{obs}}{E_{clear}}$ is 1 and CLD is zero. As cloudiness increases this ratio becomes less than 1.

Table VI. Comparison of constant coefficient (A) and power coefficient (B) from selected cloud cover power function-type algorithms with those derived for the three Antarctic sites used in this study. The region of application for each algorithm is shown.

Source	A	B	Region of application
Kasten & Czeplak 1980	0.75	3.4	Hamburg, Germany
Davis 1995	0.674	2.854	Seattle-Tacoma airport, USA
Laevastu 1960	0.6	3	Ocean Station P
Dobson & Smith 1988	0.53	0.5	Ocean Station P & Sable Island
McMurdo Station (this study)	0.20	2.09	Antarctica
Palmer Station (this study)	0.37	1.43	Antarctica
Ushuaia Station (this study)	0.38	1.48	sub-Antarctica

The clear sky RT model can be used to estimate E_{clear}, assuming that the model is appropriate for the particular site. Thus, the realism of the RT model was tested by comparing the simulated irradiances with those measured during clear sky conditions. Hourly irradiance data for which concurrent cloudiness measurements showed clear sky conditions to exist were selected from the total data sets. These data consisted of 115, 53, and 100 measurements at McMurdo Station, Palmer Station and Ushuaia, respectively. Thus, only 3.2%, 2.8%, and 1.5% of the total data set at the three sites could be classified as clear sky for the time included in this study, which indicates that the sub-

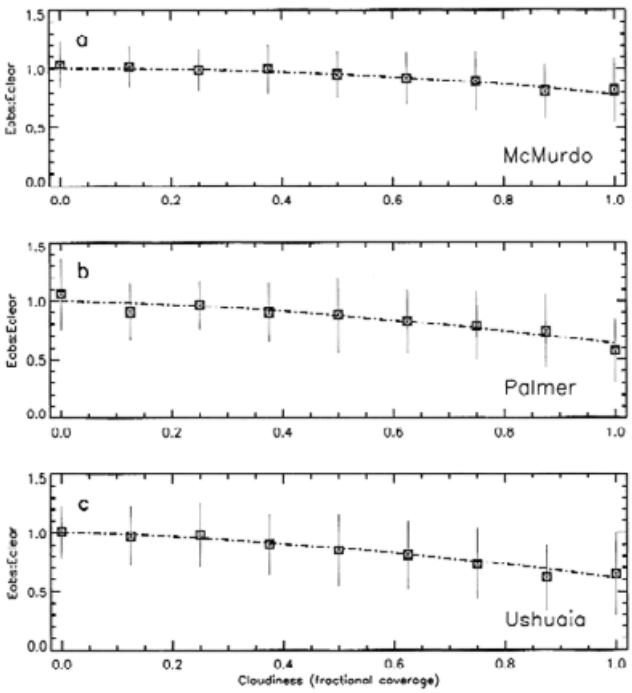

Fig. 5. The ratio of observed to simulated clear sky irradiances at **a.** McMurdo Station, **b.** Palmer Station, and **c.** Ushuaia as a function of cloudiness. The one standard deviation is shown for the observations at a given level of cloudiness. The dash-dot line shows the function fit to these data. The functional fit was derived using the cloudiness points between 0.1 to 1.0 because cloudiness of zero is not allowed in logarithmic transformation.

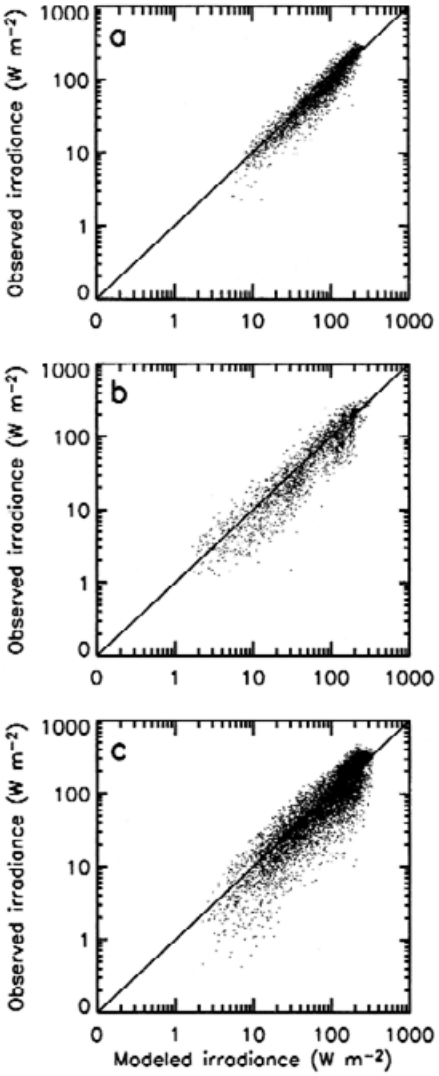

Fig. 6. Comparison between observed and simulated spectrally-integrated irradiances for **a.** McMurdo Station, **b.** Palmer Station, and **c.** Ushuaia. The irradiance values were integrated over 280 to 620 nm. Solid line represents 1:1 line. The simulated irradiances were obtained from the RT model that included a correction for cloud cover effects.

Antarctic and Antarctic sites used in this study are persistently cloudy.

The RT model was used to obtain simulated irradiances at the three sites using meteorological conditions that were concurrent with the irradiance measurements. Average ground albedos of 0.76, 0.60, and 0.38, which were calculated from the reflectivity measurements, were used as input parameters for times when measurements were not available at McMurdo Station, Palmer Station, and Ushuaia, respectively.

Comparisons between the simulated irradiances and the clear sky observations at the three sites showed excellent agreement (Fig. 4), with correlation coefficients of 0.99 for McMurdo and Palmer Stations and 0.98 at Ushuaia. Thus,

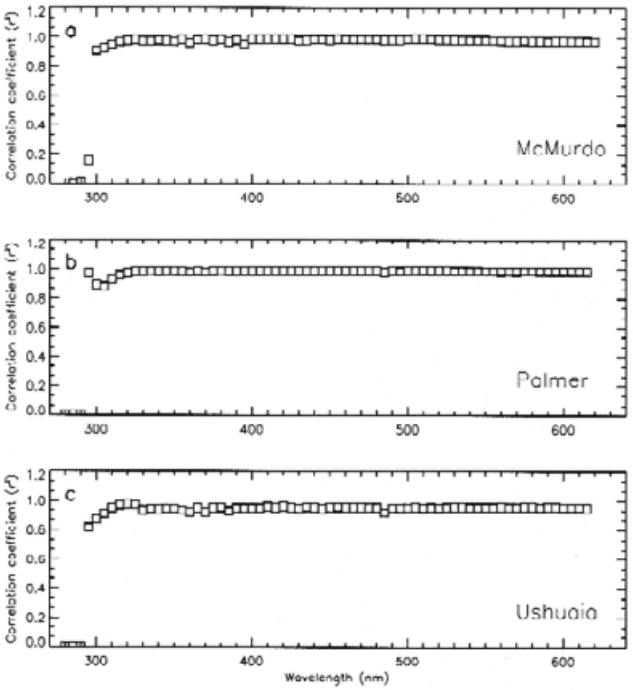

Fig. 7. Wavelength-dependent correlation coefficients ($r^2(\lambda)$) obtained from liner regression between observed and simulated irradiances for clear sky conditions at **a.** McMurdo Station, **b.** Palmer Station, and **c.** Ushuaia.

the linear relationships derived for each site (slope and constant, Fig. 4) can be used to estimate observed irradiances for clear sky conditions (E_{clear}) from the simulated values obtained from the RT model.

At McMurdo Station, Palmer Station, and Ushuaia there were 3591, 1922 and 6870 hourly irradiance observations, respectively, that also had concurrent cloudiness measurements. These data were binned according to cloudiness (in tenths) and the spectrally-resolved irradiances were integrated over 280 to 620 nm. The integrated irradiance values were then fitted with a power function of the form given in Eq. (5) to obtain the coefficients A and B at the three sites (Table VI). The constant coefficients (A) estimated for McMurdo Station, Palmer Station, and Ushuaia were 0.20, 0.37, 0.38, respectively. The power coefficient (B) estimated for the three sites was 2.1 for McMurdo Station, 1.4 for Palmer Station, and 1.5 for Ushuaia (Table VI). The coefficient sets obtained for Palmer Station and Ushuaia are similar; whereas, those obtained for McMurdo Station showed a lower constant coefficient and about a 50% higher power coefficient. The constant coefficients (A) estimated for the sub-Antarctic and Antarctic sites were about two-fold lower than those estimated for mid-latitude areas (Table VI). The power coefficients (B) estimated for the sub-Antarctic and Antarctic sites were lower than those obtained from other studies (Table VI).

As cloudiness increases, the ratio of observed to clear sky

irradiances, $\frac{E_{obs}}{E_{clear}}$, decreases. The ratio values computed for various cloudiness values show this decrease (Fig. 5) and at fully overcast conditions the mean ratio values are 0.82, 0.57, and 0.64 for McMurdo Station, Palmer Station, and Ushuaia, respectively. The mean ratio for overcast conditions was highest at McMurdo Station, which implies that this southernmost site is influenced by multiple reflection more than the other two stations. The agreement between integrated irradiance observations and the simulated irradiances from the RT model that uses the newly estimated cloud cover algorithm coefficients for the three sites (Table VI) is good (Fig. 6). The simulated irradiances from Ushuaia (Fig. 6c) showed the largest scatter among the three sites, and the scatter increases with higher irradiance values. This scatter is related to the standard deviation of the observations at each cloudiness condition (Fig. 5c), which increases at Ushuaia as cloudiness increases.

Derivation of new algorithms for spectrally-resolved irradiance

The cloud cover correction algorithm given by Eq. (5) is based on the integrated irradiance between 280–620 nm. However, the spectral properties of the clouds can modify the irradiance with respect to wavelength. This spectral effect is described by a cloud cover correction algorithm of the form:

$$\frac{E_{obs}(\lambda)}{E_{clear}(\lambda)} = 1 - A(\lambda)\cdot(CLD)^{B(\lambda)} \qquad (6)$$

where the coefficients $A(\lambda)$ and $B(\lambda)$ are the same as in Eq. (5), but are now functions of wavelength, λ.

The irradiance data used in this calculation were based on the wavelengths between 280 and 620 nm at 1 nm intervals for McMurdo Station, Palmer Station, and Ushuaia. These data were then fit with Eq. (6) to obtain spectrally-resolved estimates of the the coefficients $A(\lambda)$ and $B(\lambda)$ as follows.

The spectrally-resolved correlation coefficients ($r^2(\lambda)$) calculated between the observed and simulated irradiances for clear sky conditions at the three sites (Fig. 7) show essentially a linear relationship between observed and simulated irradiances at wavelengths greater than 300 nm, which include the ultraviolet-A (UV-A) and photosynthetically available radiation (PAR) portions of the light spectra. The lack of a strong correlation at shorter wavelengths (280–300 nm) at all three sites (Fig. 7) suggests that the RT model does not correctly simulate clear sky irradiances in some parts of the UV-B (280–320 nm) region. However, the possibility that the measurements are not reliable for wavelengths shorter than 295–298 nm cannot be excluded because the actual spectral irradiances are at the noise level of the detector for wavelengths shorter than 295 nm (Lubin *et al.* 1992). Additionally, the irradiance

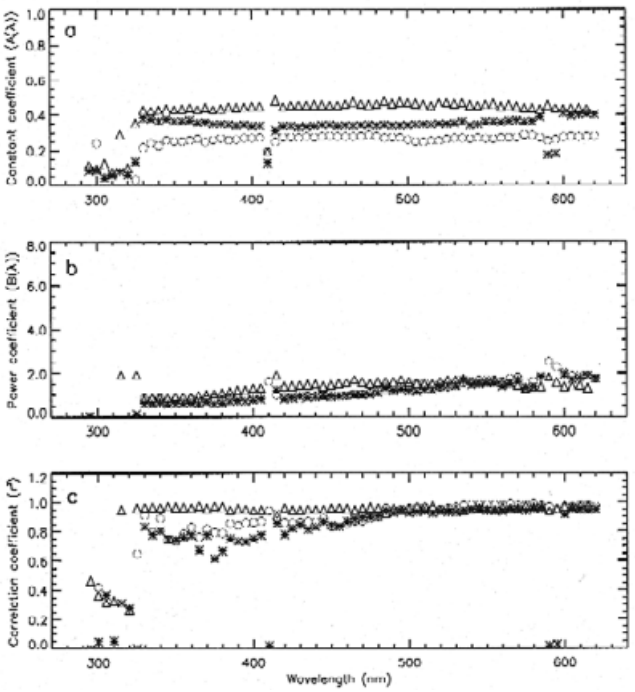

Fig. 8. Wavelength-dependent estimates of the **a.** constant coefficient, $A(\lambda)$, **b.** power coefficient, $B(\lambda)$ derived for cloud cover correction algorithms at McMurdo Station (O), Palmer Station (*), and Ushuaia (D), and **c.** wavelength-dependent correlation coefficients ($r^2(\lambda)$) derived from comparisons between observed and simulated irradiances for all cloudiness conditions at the three sites.

flux in the UV-B portion of the spectra is much smaller than in the visible, thereby allowing any absolute error to have a large influence.

The linear relationships allow the wavelength-dependent clear-sky irradiances to be predicted from the RT model at wavelengths greater than 300 nm. These values can be used with observations obtained for different cloudiness conditions to compute the ratio, $\frac{E_{obs}(\lambda)}{E_{clear}(\lambda)}$. This is the same approach used for the integrated irradiance values above, but with the wavelength-dependent information retained. Equation (6) was fitted to the spectrally-resolved hourly irradiance observations, binned according to cloudiness, for the three sites to derive values of $A(\lambda)$ and $B(\lambda)$ with respect to wavelength.

The minimum value of $A(\lambda)$ was obtained for McMurdo Station and the maximum was obtained for Ushuaia (Fig. 8a). With few exceptions the value of this coefficient converged to a constant value for wavelengths greater than 330 nm. The changes in the value of $A(\lambda)$ at all wavelengths were minimal. The values of $A(\lambda)$ obtained at McMurdo Station and Palmer Station are similar to those obtained for the spectrally-averaged irradiances, especially for $\lambda >$ 330 nm. For example, $A(\lambda)$ averaged over 330 to 620 nm is 0.26 for McMurdo Station, 0.34 for Palmer Station, and 0.44 for Ushuaia, respectively. These values are similar to

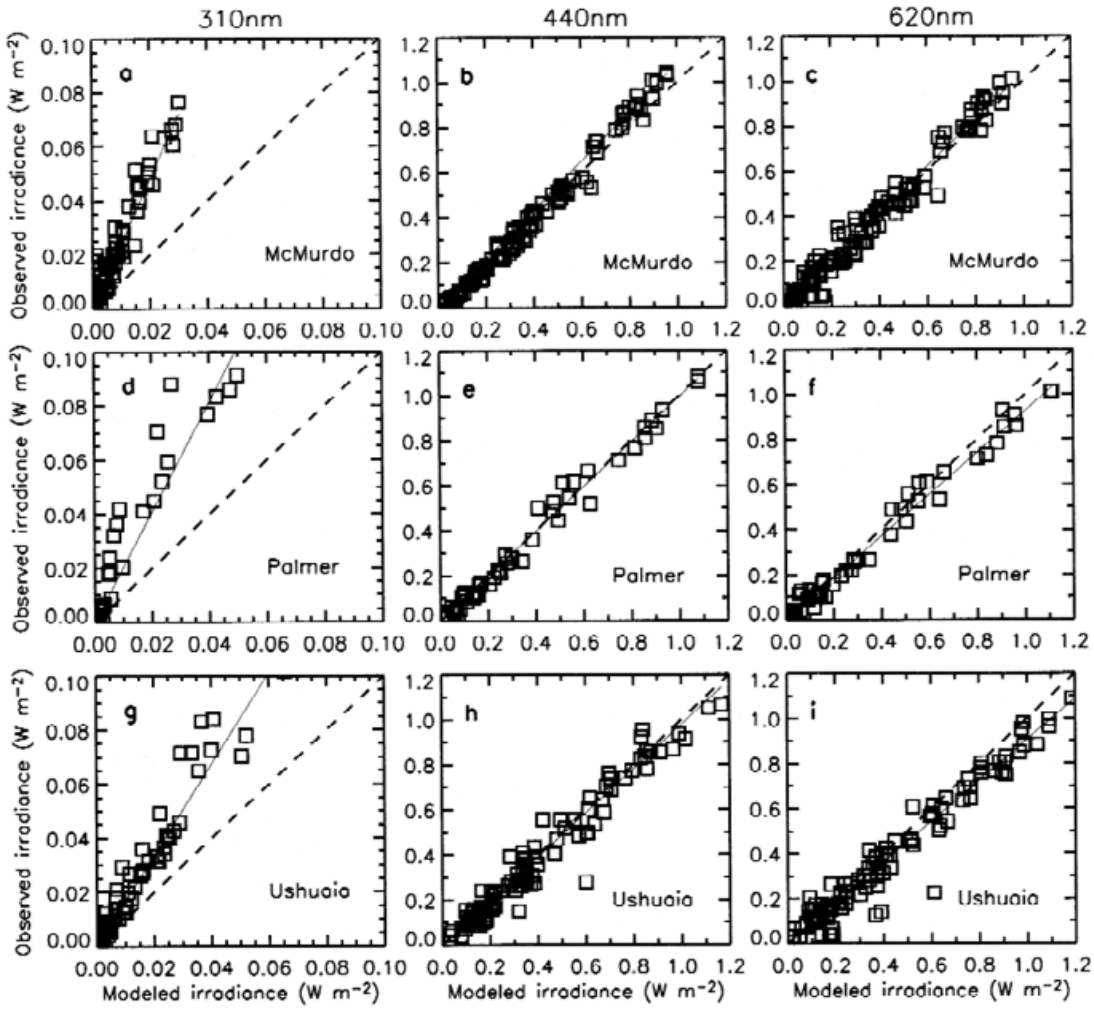

Fig. 9. Comparisons between observed and simulated irradiances at three wavelengths at **a–c.** McMurdo Station, **d–f.** Palmer Station, and **g–i.** Ushuaia. The linear regression between the observed and simulated irradiances is given by the solid line and the 1:1 correspondence line, given for reference, is shown as a dashed line.

spectrally-averaged coefficient values estimated for the three sites (Table VI). The values of $B(\lambda)$ obtained for the three sites were similar across all wavelengths (Fig. 8b). The $B(\lambda)$ values for $\lambda > 330$ nm for the three sites are lower than those obtained using the spectrally-averaged irradiance data (Table VI), 1.25 for McMurdo Station and 1.01 for Palmer Station, and 1.37 for Ushuaia, respectively. The correlation coefficient between the observed and simulated irradiances, using the new $A(\lambda)$ and $B(\lambda)$ values, is significant at the three sites for irradiances at wavelengths greater than 330 nm (Fig. 8c). These results allow extrapolation of $A(\lambda)$ and $B(\lambda)$ from 620 nm to 700 nm to include the whole range of PAR (400–700 nm).

Comparisons between the observed and simulated irradiances at three wavelengths for the three sites (Fig. 9) show good agreement for three representative wavelengths. At short wavelengths (e.g. 310 nm), the simulated irradiances tend to underestimate observed values. However, the model-observation comparisons tend to follow the 1-to-1 line for longer wavelengths (440 and 620 nm).

Discussion

Parameter sensitivity and new cloud cover correction algorithms

Gregg & Carder (1990) suggest that air mass type, visibility and ozone concentration are the meteorological input parameters that have the most effect on simulated irradiance fields obtained from the RT model. In this study, visibility and ozone concentration also were identified as having the most influence on simulated irradiances. Air mass type was not varied in this study. The sensitivity to visibility and ozone concentration differed from that obtained by Gregg & Carder (1990), which was 12.0% and 7.0%, respectively, because of the differing parameter ranges and differing solar zenith angles used in this study. The parameter range for visibility used by Gregg & Carder (1990) was 5–25 km,

which is less than that used in this study (Table II). The effect of ozone concentration is more pronounced at high latitude where there is a larger atmospheric path length due to the high solar zenith angle. Gregg & Carder (1990) used a solar zenith angle of 60°, whereas, that for McMurdo Station is 80°. This results in the higher sensitivity of the simulated irradiances to ozone concentration in this study. Reflectivity was also identified in this study as having a strong influence on the simulated irradiances, especially at sites like McMurdo Station which has a large solar zenith angle.

The comparisons of the empirical coefficients, A and B, derived for the sub-Antarctic and Antarctic sites with those derived for other regions (Table VI) show considerable differences. The values obtained for A at the three sites are 2-fold less than those from all the mid-latitude sites. Because A is related to the slope of the line (Eq. 5) this suggests that the effect of cloud cover on the irradiance ratio, $\frac{E_{obs}}{E_{clear}}$, is less significant for the Antarctic sites than for the mid-latitude sites. Comparison of the value of A among the sub-Antarctic and Antarctic sites shows that the slope decreases as latitude increases (Table VI), which indicates that higher latitudes are more influenced by multiple reflections between the ground and bottom of the clouds (Fig. 2a).

The values of B estimated for the sub-Antarctic and Antarctic sites are also less than those obtained for mid-latitude locations (Table VI), which indicates that the curvature (Fig. 5) is reduced for high latitude regions relative to mid latitudes. The implication is that the cloud cover effect at high latitudes, at least for Palmer Station and Ushuaia, is approximately linearly related to the two-dimensional fractional cloud cover. This supports the use of a two-dimensional cloud cover correction approximation for high latitude regions where stratus clouds prevail and vertically developed convective clouds are scarce thereby reducing the importance of three-dimensional cloud effects (Ricchiazzi & Gautier 1998). This is not the case for McMurdo Station which has the highest $B(\lambda)$ value (2.09) estimated for the three sites. However, this value is still less than that estimated for mid latitudes (Table VI). Interestingly, the value of B estimated for McMurdo Station is close to the one obtained for the Seattle, WA region, which experiences considerable cloudiness throughout the year. The fraction of cloudy days (50% of sky is covered) in the total observations is similar between the two sites, 60% for Seattle, WA (Davis 1995) versus 67% for McMurdo Station.

The newly derived values of A and B differ from those reported for other regions (Table VI) and also are greater than the theoretical value of 1.0 for B, which occurs when cloud type and fractional change in cloud cover are the same. In this case, the radiant energy flux is linearly related to cloud cover. However, two factors can make B larger than 1.0. First, the observed cloudiness, expressed in oktas or tenths, is often biased because observers report values that are too high relative to other measures such as those obtained from satellites. Satellite or lidar observations look straight down or up, respectively, which determine for a specific point on Earth only clouds or no clouds. By averaging in time and space, mean values are obtained. However, cloud observations by an observer include the whole sky, and estimate the mean cloudiness for a specific point. To an observer looking toward the horizon, cloud cover appears more extensive than it actually is, which introduces bias into the observation. As a result, near clear or near totally cloudy conditions are usually measured accurately, but intermediate cloudiness values contain more subjectivity. Second, often, as the cloud fraction increases, so does the vertical extent of clouds, so that they become thicker as cloud cover approaches full cloudiness, which appears as more extensive cloud cover than actual conditions. These observations give higher values, as clouds also have a vertical dimension, which leads to an overestimation of broken cloudiness when compared to the satellite or lidar observations.

The values of B estimated from this study for Palmer Station and Ushuaia are 1.43 and 1.48, respectively. These values suggest that the fractional cloud cover measurements from these sites are reliable and that the two-dimensional assumption of the cloud cover correction algorithm is applicable to these areas for making comparisons of integrated irradiance values. The value of B obtained for McMurdo Station exceeds the theoretical value of 1.0 by 110%, which suggests that observer bias may have occurred or that cloud type and fractional change in cloud cover may have not been the same.

The comparisons shown in Table VI illustrate the importance of intercalibration of cloud cover correction algorithms derived for various locations and point to the need to develop these for specific regions. Also, RT models that include effects of multiple reflections between the surface and the bottom of clouds on the diffuse and direct components of irradiance are needed.

The irradiance ratio, $\frac{E_{obs}}{E_{clear}}$, for fully overcast skies for mid-latitudes is between 0.4 and 0.6 (Lubin & Frederick 1991). The ratio values obtained for Palmer Station and Ushuaia are 0.57, and 0.64, respectively, which are at the upper limit of this range (Fig. 5). Lubin & Frederick (1991) estimated a value of 0.44 for this ratio at Palmer Station, which differs from the ratio value obtained in this study. The Lubin & Frederick (1991) value is lower because sea ice concentration during the time the estimate was made (1988/1989) was less than the climatological average (Stammerjohn & Smith 1996), which reduces the multiple reflections between sea ice and clouds. The ratio value obtained for McMurdo Station is higher (0.79). However, the comparisons between simulated clear sky irradiances and observed values (Fig. 2) show that measured irradiances at McMurdo Station are affected by cloud cover

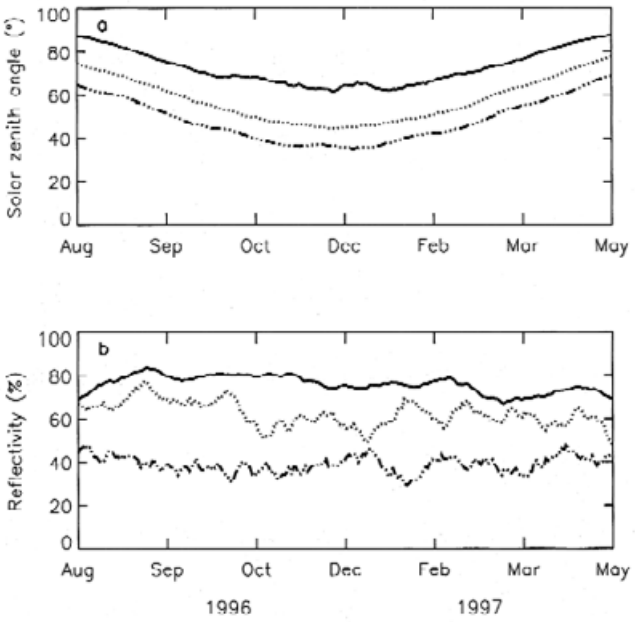

Fig. 10. Time series of **a.** solar zenith angle and **b.** reflectivity measured at McMurdo Station (—), Palmer Station (• • •), and Ushuaia (- • • -) for the time included in this study.

and multiple reflections (a high albedo), which is manifest in the higher value obtained for the cloudiness factor at this site.

McMurdo Station differences in daily-averaged irradiance

McMurdo Station is located at a high latitude and, as a result, the solar zenith angle at this site is large relative to the two other sites (Fig. 10a). McMurdo Station also has higher reflectivity than Palmer and Ushuaia Station (Fig. 10b). Thus, one explanation for the underestimation of the irradiance values at McMurdo Station by the RT model is that, although the modified RT model includes albedo (reflectivity) effects, it does not include multiple reflections between the bottom of the clouds and the high albedo surface. Multiple reflections between the ground surface and the bottom of the clouds is important, especially for a highly reflective surface (Nann & Riordan 1990, Wendler *et al.* 2004), and can increase the measured solar radiation by a factor of 2 or more in overcast conditions (Gardiner 1987).

Another explanation for the underestimation of the daily-averaged irradiances at McMurdo Station is mismatches in the data sets that are input to the RT model. The meteorological measurements used with the RT model are either monthly-averaged or climatological values, whereas, the irradiance measurements are daily averaged. Also, the cloud cover estimates were obtained by averaging and integrating measurements that are obtained at irregular and infrequent time intervals at this site. The latter may have a large effect because cloud cover is a primary factor influencing the irradiance arriving at the surface.

Short wavelength radiation issues

The simulated irradiances obtained with the RT model compared poorly with observed irradiances for wavelengths shorter than 330 nm at all three sites (cf. Fig. 9). The simulated values consistently underestimate observed irradiances. This mismatch is illustrated by the slope of the linear regression between the observed and simulated irradiances (Fig. 11). The slope decreases asymptotically to 1 as wavelength gets longer, with this being most pronounced at McMurdo Station. This indicates that the simulated irradiances are lower than observed values for clear sky conditions at a given wavelength.

The clear sky RT model provides realistic simulations (r^2 > 70%) of irradiance for wavelengths between 330–620 nm with a few exceptions at the three sites (Fig. 8c). The implication is that the empirical power function cloud cover correction algorithm is not applicable for wavelengths between 280–320 nm at these sites.

One possible explanation for the problem at short wavelengths is multiple reflection between the bottom of the clouds and the ground and/or sea surface. Multiple reflection of photons between a cloud base and a snow or ice surface can vary the shortwave surface irradiance significantly, often doubling the downwelling irradiance relative to an open ocean surface (Gardiner 1987).

According to Bartlett *et al.* (1998), clouds are generally white or light grey in colour, and downwelling irradiance that passes through the cloud and reaches the Earth's surface is then reflected with a reflectivity determined by the ground albedo, yielding upwelling irradiance. Part of the upwelling irradiance is then reflected off the spectrally neutral bottom surface of the overlaying clouds, yielding downwelling irradiance. This multiple reflection process is spectrally neutral and simply increases the magnitude of the downwelling irradiance. Part of this reflected irradiance is then scattered back toward the Earth's surface by atmospheric constituents. The scattering is greater at shorter (blue) wavelengths than at longer (red) wavelengths, so the resulting downwelling irradiance is shifted to shorter wavelengths relative to irradiance under clear sky conditions (Bartlett *et al.* 1998). These processes are not included in the RT model used in this study. A recent study by Wendler *et al.* (2004) describes the effect of multiple reflection and albedo on the net radiation in Antarctica and shows that the net radiation was a strong function of both fractional cloud cover and surface albedo. Wendler *et al.* (2004) found that incoming global radiation was higher under overcast conditions than for clear sky conditions when a highly reflecting surface was present.

The RT model used the surface albedo measured at one wavelength. However, the effect of surface albedo on the irradiance (especially, on the UV part of the light spectrum)

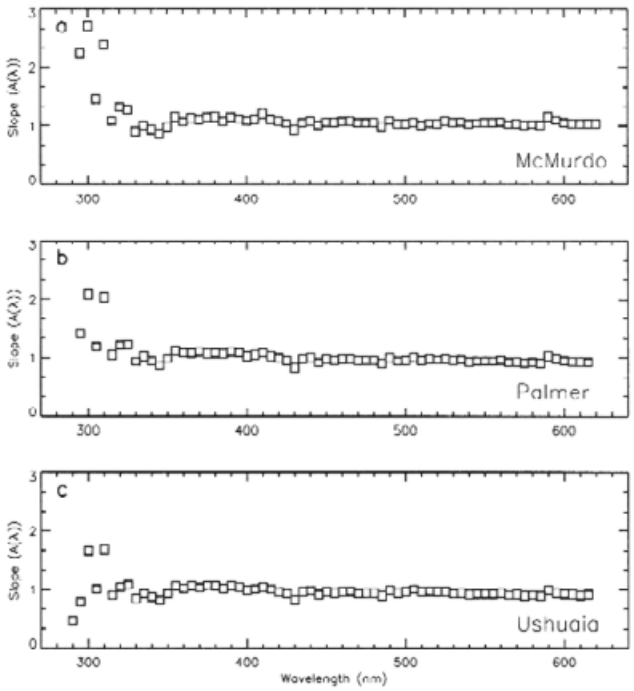

Fig. 11. Wavelength-dependent slope obtained from linear regression between observed and simulated irradiances for clear sky conditions at **a.** McMurdo Station, **b.** Palmer Station, and **c.** Ushuaia.

can be wavelength-dependent as a result of multiple reflection (Smith *et al.* 1992). The snow albedo, in particular, is variable at short wavelengths depending on the snow condition (Wiscombe & Warren 1980, Grenfell *et al.* 1994). Therefore, the surface albedo effects on the UV-B portion of the irradiance spectrum may have been strong. The behaviour of model in the short wavelengths can be improved by explicit inclusion of the multiple reflection process.

Cloud issues

In this study, the effect of cloud type on the radiant flux was not considered. Variation of cloud type can be as important as fractional cloud coverage in changing the magnitude and spectral shape of the radiant flux (Chen *et al.* 2000). Exclusion of the effect of the three-dimensional morphology of clouds in this study could explain some of the differences in the simulated irradiances and measurements for cloudy conditions. Clouds in high latitude regions have limited vertical extensions and conform to an idealized plane-parallel stratiform structure (Lubin & Frederick 1991), but these characteristics may not be always persistent. The cloud types most frequently observed at the three sites used for this study were low-level clouds, such as stratus (St) and stratocumulus (Sc), and mid-level clouds, such as nimbostratus (Ns), altostratus (As) and altocumulus (Ac). Analysis of the cloud type observations shows little variation in seasonal and spatial characteristics at the three sites throughout the year.

However, the microphysical properties of clouds will affect the magnitude and shape of the radiant flux. This represents a potentially important processes that affects radiant fluxes at high latitudes (Saxena & Ruggiero 1990). However, inclusion of such detail in RT models must await observations that allow parameterization of the processes.

Generalizations

The cloud cover correction algorithms derived for the sub-Antarctic and Antarctic sites used in this study can be generalized for application to other areas of the Southern Ocean. The constant coefficients ($A(\lambda)$) derived for the three sites show a regional dependence and the spectral dependency of this coefficient is neutral for wavelengths larger than 330 nm (Fig. 8a). Thus, a value of A could be estimated for a range of latitudes between 55° and 78° using the trends in the spectrally-averaged values of A (Table VI) obtained from this study. This could then be used for $A(\lambda)$ for $\lambda > 330$ nm.

The regional dependency of $B(\lambda)$ is not as strong as that for $A(\lambda)$ (Fig. 8b vs. 8a). However, the same trend is suggested by the spectrally-averaged value of B (Table VI). The spectral dependency of $B(\lambda)$ is also neutral at > 330 nm (Fig. 8b). Thus, values for this coefficient for a range of locations in the Antarctic could also be estimated, similar to the approach used for A.

Values of $A(\lambda)$ and $B(\lambda)$ for wavelengths between 330–400 nm should be determined for individual sites. The results from this study suggest that these cannot be generalized for the entirety of the Southern Ocean.

Conclusions

Comparisons between simulated and observed irradiances for one sub-Antarctic and two Antarctic sites were done to assess existing cloud cover correction algorithms in an attempt to develop an approach for estimating surface irradiance fields. The coefficient sets (A and B) derived for power function cloud cover correction algorithms for the three sites had smaller ranges than those obtained for mid latitudes, which indicates the influence of multiple reflection between the bottom of clouds and high surface albedo. The coefficient sets derived in this study showed regional variation depending on locations and no spectral dependency of the coefficient sets was found for $\lambda >$ 330 nm, which implies that the spectral effect of cloud cover is neutral over the range of PAR. The regional dependency of the coefficient sets over the range of PAR produces an approach for extending cloud cover correction algorithms to other areas of the Antarctic.

The application of satellite-based cloud cover measurements to estimate surface irradiance, especially, at

high latitudes where it is difficult to distinguish between cloud and ice cover signals, is limited. Also, the limited time span of satellite-derived irradiance measurements, about two decades, makes it difficult to use these with historical biological data sets to estimate quantities such as primary production. The present study, which uses a RT model with a cloud cover correction algorithm, provides an approach for obtaining irradiance fields prior to the availability of satellite measurements. It is also an approach for validating satellite-derived irradiance fields.

More accurate estimation of UV-B by the RT model is needed to study environmental issues associated with increased UV radiation over Antarctica resulting from ozone depletion. Also, the multiple reflection effect between the bottom of the clouds and high albedo surfaces needs to be included to improve the cloud cover correction algorithms and RT model simulations. Inclusion of wavelength-dependent albedos for different surfaces, such as open ocean, old and new snow, and ice types, in the RT model will improve the skill of the model at high latitude coastal sites. Inter-calibration between sites and between land-based and satellite-based observations is important to remove ambiguity in measurements. Removal of the ambiguity in the signals coming from both the ground with high albedo surface and the top of the cloud will allow the remotely assessed albedo and cloud information to be used for more accurate estimates of surface radiant fluxes at a large scale.

Acknowledgements

We thank Drs John Klinck and Chester Grosch for helpful and constructive comments and advice throughout this study. Comments provided by Dr G. Wendler, one anonymous reviewer and Dr M. van den Broeke were most helpful in writing and revising this manuscript. We also thank Biospherical Instruments Inc. for providing the irradiance data sets for the three sites and manuals explaining the measurements protocols. This research was supported by the U.S. National Science Foundation, Office of Polar Programs grant numbers OPP-9618383, OPP-9909956, and OPP-0087690. Computer resources and facilities were provided by the Center for Coastal Physical Oceanography at Old Dominion University.

References

Antoine, D. & Morel, A. 1996. Oceanic primary production 1. Adaptation of a spectral light-photosynthesis model in view of application to satellite chlorophyll observations. *Global Biogeochemical Cycles*, **10**, 43–55.

Antoine, D., Andre, J. & Morel, A. 1996. Oceanic primary production 2. Estimation at global scale from satellite (coastal zone color scanner) chlorophyll. *Global Biogeochemical Cycles*, **10**, 57–69.

Bartlett, J., Ciotti, A., Davis, R. & Cullen, J. 1998. The spectral effects of clouds on solar irradiance. *Journal of Geophysical Research*, **103**, 31 017–31 031.

Bird, R. & Riordan, C. 1985. Simple solar spectral model for direct and diffuse irradiance on horizontal and tilted planes at the earth's surface for cloudless atmospheres. *Journal of Climate and Applied Meteorology*, **25**, 87–97.

Bishop, J.K.B. & Rossow, W.B. 1991. Spatial and temporal variability of global surface solar irradiance. *Journal of Geophysical Research*, **96**, 16 839–16 858.

Bishop, J.K.B., Rossow, W.B. & Dutton, E.G. 1997. Surface solar irradiance from the International Satellite Cloud Climatology Project 1983–1991. *Journal of Geophysical Research*, **102**, 6883–6910.

Booth, C, Ehramjian, J., Mestechkina, T., Cabasug, L., Robertson, J. & Tusson, J. 1998. *NSF Polar Programs UV Spectroradiometer Network 1995–1997 Operations Report*. San Diego, CA: Biospherical Instruments Inc., 241 pp.

Booth, C, Bernhard, G., Ehramjian, J., Cabasug, L., Quang, V. & Lynch, S. 2000. *NSF Polar Programs UV Spectroradiometer Network 1997–1998 Operations Report*. San Diego, CA: Biospherical Instruments Inc., 231 pp.

Booth, C, Bernhard, G., Ehramjian, J., Quang, V., Lynch, S. 2001. *NSF Polar Programs UV Spectroradiometer Network 1998–1999 Operations Report*. San Diego, CA: Biospherical Instruments Inc., 6–12.

Chen, T., Rossow, W. & Zhang, Y. 2000. Radiative effects of cloud-type variations. *Journal of Climate*, **13**, 264–286.

Davis, R. 1995. Comparison of modeled to observed global irradiance. *Journal of the Applied Meteorology*, **35**, 192–201.

Dobson, F. & Smith, S. 1988. Bulk models of solar radiation at sea. *Quarterly Journal of Royal Meteorological Society*, **114**, 165–182.

Gardiner, B. 1987. Solar radiation transmitted to the ground through cloud in relation to surface albedo. *Journal of Geophysical Research*, **92**, 4010–4018.

Gautier, C, He, G., Yang, S. & Lubin, D. 1994. Role of clouds and ozone on spectral ultraviolet-B radiation and biologically active UV dose over Antarctica. *Antarctic Research Series*, **62**, 83–91

Green, A. & Chai, S. 1988. Solar spectral irradiance in the visible and infrared regions. *Photochemistry and Photobiology*, **48**, 477–486.

Gregg, W. & Carder, K. 1990. A simple spectral solar irradiance model for cloudless maritime atmospheres. *Limnology and Oceanography*, **35**, 1657–1675.

Grenfell, T., Warren, S., & Mullen, P. 1994. Reflection of solar radiation by the Antarctic snow surface at ultraviolet, visible, and near-infrared wavelengths. *Journal of Geophysical Research*, **99**, 18 669–18 684.

Justus, C. & Paris, M. 1985. A model for solar spectral irradiance at the bottom and top of a cloudless atmosphere. *Journal of Climate and Applied Meteorology*, **24**, 193–205.

Kasten, F. & Czeplak, G. 1980. Solar and terrestrial radiation dependent on the amount and type of cloud. *Solar Energy*, **24**, 177–189.

Laevastu, T. 1960. Factors affecting the temperature of the surface layer of the sea. *Commentativeness Physico-Mathematicae*, **25**, 1–136.

Leckner, B. 1978. The spectral distribution of solar radiation at the earth's surface-elements of a model. *Solar Energy*, **20**, 143–150.

Lubin, D. & Frederick, J.E. 1991. The ultraviolet radiation environment of the Antarctic Peninsula: the roles of ozone and cloud cover. *Journal of Applied Meteorology*, **30**, 478–493.

Lubin, D., Mitchell, B.G., Frederick, J.E., Alberts, A.D., Booth, C.R., Lucas, T. & Neuschuler, D. 1992. A contribution toward understanding the biospherical significance of Antarctic ozone depletion. *Journal of Geophysical Research*, **97**, 7817–7828.

Molina, L. & Molina, M. 1986. Absolute absorption cross sections of ozone in the 185- to 350-nm wavelength range. *Journal of Geophysical Research*, **91**, 14 501–14 508.

NANN, S. & RIORDAN, C. 1990. Solar spectral irradiance under clear and cloudy skies: measurements and a semiempirical model. *Journal of Applied Meteorology*, **30**, 447–462.

NCDC. 2003. *National Climatic Data Center Data Documentation for Data Set 3505* (*DSI-3505*), *Integrated Surface Hourly Data.* Asheville, NC: National Climatic Data Center, 62 pp.

O'HIROK, W & GAUTIER, C. 1998a. A three-dimensional radiative transfer model to investigate the solar radiation within a cloudy atmosphere. Part I: Spatial effects. *Journal of Atmospheric Science*, **55**, 2162–2179.

O'HIROK, W. & GAUTIER, C. 1998b. A three-dimensional radiative transfer model to investigate the solar radiation within a cloudy atmosphere. Part II: Spectral effects. *Journal of Atmospheric Science*, **55**, 3065–3076.

REED, R. 1977. On estimating insolation over the ocean. *Journal of Physical Oceanography*, **7**, 482–485.

REIFSNYDER, W. & LULL, H. 1965. Radiant energy in relation to forests. *Technical Bulletin No.1344*. Washington, DC: US Department of Agriculture, 17 pp.

RICCHIAZZI, P. & GAUTIER, C. 1998. Investigation of the effect of surface heterogeneity and topography on the radiation environment of Palmer Station, Antarctica, with a hybrid 3-D radiative transfer model. *Journal of Geophysical Research*, **103**, 6161–6176.

RICCHIAZZI, P., YANG, S., GAUTIER, C. & SOWLE, D. 1998. SBDART: a research and teaching software tool for plane-parallel radiative transfer in the Earth's atmosphere. *Bulletin of the American Meteorological Society*, **79**, 2101–2114.

SAXENA, V. & RUGGIERO, F. 1990. Antarctic coastal stratus clouds: microstructure and acidity. *Antarctic Research Series*, **50**, 7–18.

SCHAFER, J., SAXENA, V., WENNY, B., BARNARD, W. & DE LUISI, J. 1996. Observed influence of clouds on ultraviolet-B radiation. *Geophysical Research Letters*, **23**, 2625–2628.

SECKMEYER, G., ERB, R. & ALBOLD, A. 1996. Transmittance of a cloud is wavelength-dependent in the UV-range. *Geophysical Research Letters*, **23**, 2753–2755.

SIEGEL, D. & DICKEY, T. 1987. On the parameterization of irradiance for open ocean photoprocesses. *Journal of Geophysical Research*, **92**, 14 648–14 662.

SIEGEL, D., WESTBERRY, T. & OHLMANN, J. 1999. Cloud color and ocean radiant heating. *Journal of Climate*, **12**, 1101–1116.

SMITH, R., WAN, Z. & BAKER, K. 1992. Ozone depletion in Antarctica: modeling its effect on solar UV irradiance under clear-sky conditions. *Journal of Geophysical Research*, **97**, 7383–7397.

SPINHIRNE, J. & GREEN, A. 1978. Calculation of the relative influence of cloud layers on received ultraviolet and integrated solar radiation. *Atmospheric Environment*, **12**, 2449–2454.

STAMMERJOHN, S. & SMITH, R. 1996. Spatial and temporal variability of western Antarctic Peninsula sea ice coverage. *Antarctic Research Series*, **70**, 81–104.

TABATA, S. 1964. Insolation in relation to cloud amount and sun's altitude. *In Studies on Oceanography*. Seattle, WA: University of Washington Press, 202–210.

WENDLER, G., MOORE, B., HARTMANN, B., STUEFER, M. & FLINT, R. 2004. Effects of multiple reflection and albedo on the net radiation in the pack ice zones of Antarctica. *Journal of Geophysical Research*, **109**, doi: 10.1029/2003JD003927.

WISCOMBE, W. & WARREN, S. 1980. A model for the spectral albedo of snow. I: Pure snow. *Journal of the Atmospheric Sciences*, **37**, 2712–2733.